Millimeter-Wave Transmission for Small-Cell Backhaul in Dense Urban Environment: a Solution Based on MIMO-OFDM and Space-Time Shift Keying (STSK)

**CLAUDIO SACCHI[1], (Senior Member, IEEE), TALHA FAIZUR RAHMAN[1],
IBRAHIM A. HEMADEH[2], AND MOHAMMED EL-HAJJAR[2], (Senior Member, IEEE)**
[1]Department of Information Engineering and Computer Science, University of Trento, I-38123 Trento, Italy
[2]Department of Electronics and Computer Science, University of Southampton, SO17 1BJ Southampton, U.K.

Corresponding author: C. Sacchi (claudio.sacchi@unitn.it)

ABSTRACT Next generation wireless standards will exploit the wide bandwidth available at the millimeter-wave (mm-Wave) frequencies, in particular the *E*-band (71–76 and 81–86 GHz). This large available bandwidth may be converted into multi-gigabit capacity, when efficient and computationally affordable transceivers are designed to cope with the constrained power budget, the clustered fading, and the high level of phase noise, which actually characterize mm-wave connections. In this paper, we propose a viable multiple-input multiple-output (MIMO) solution for high bit-rate transmission in the *E*-band with application to small-cell backhaul based on space-time shift keying (STSK) and orthogonal frequency division multiplexing. STSK provides an efficient tradeoff between diversity and multiplexing without inter-channel interference and without the need for large antenna arrays. These features make STSK theoretically preferable over other throughput-oriented space-time coding techniques, namely, spatial multiplexing and spatial modulation, which were recently considered in the literature for mm-wave MIMO applications. In this paper, we consider the most significant channel impairments related to small-cell backhaul in dense urban environment, namely, the correlated fading with and without the presence the line-of-sight, the phase noise, the rain attenuation, and shadowing. In addition, we consider small-size MIMO systems (2 × 2 and 4 × 4), and low-cost base station equipments in the perspective of easily deployable small-cell network components. Comparative results, obtained by intensive simulations targeted at assessing link performance and coverage, have clearly shown the superior performance of STSK against counterpart techniques, although obtained at the cost of a somewhat reduced spectral efficiency.

INDEX TERMS Millimeter wave communications, MIMO, OFDM, space-time coding, space-time shift keying, small cells, wireless backhaul, 5G.

I. INTRODUCTION

As stated in [1], the key essence of 5G wireless networks lies in exploring the unused high frequency millimeter-wave (mm-wave) bands, formally ranging from 3 to 300 GHz. Even a small fraction of the available mm-wave spectrum can support data rate that is hundred times that in current cellular spectrum.

Hence, the use of the E-band for short and medium range point-to-point terrestrial communications has been recently considered worldwide [2]. For example, the Federal Communications Commission (FCC) has regulated the use of frequencies at E-band from 71 GHz to 76 GHz, from 81 GHz to 86 GHz and from 92 GHz to 95 GHz to licensed users in 2003. In Europe, the Electronic Communication Committee (ECC) has recommended through the ECC/REC (05)/07 such frequency bands for broadband fixed radio link applications. A document issued in 2008 by the Ministry of Economic Development of Australia contains some preliminary regulations on the usage of the E-bands for terrestrial wireless communications. As alternative to the E-band, recent licensing process of the 28 GHz band pointed out the possibility of using the frequency range from

27.50 GHz to 28.35 GHz, which can be organized into two slots of 360 MHz each [3].

The rigorous and detailed experimental analysis of mm-wave propagation proposed in [4] estimated the achievable capacity in dense urban environment both in the presence and absence of LOS, where sounders equipped with small-size antenna arrays of 4 and 8 elements have been used for practical tests in New York City. Results were shown for 73 GHz E-band compared to 28 GHz band, while considering the same channelisation of 500 MHz. The outcomes of the aforementioned analysis showed that the higher pathloss measured at 73 GHz limits the available cell-edge rate, which is approximately half of the capacity achieved in the 28 GHz band, while using the same number of antenna elements. However, using twice the number of antennas compared to 28 GHz allows the 73 GHz transmitters (Tx) to efficiently exploit MIMO spatial diversity without increasing the array size. Due to higher pathloss, NLOS mm-wave link capacity significantly drops with respect to LOS one, but it is still 20 fold increased with respect to that of sub 6 GHz bands [4].

As reported in [4], MIMO techniques represent the first cornerstone of future multi-gigabit mm-wave communications. The second cornerstone is represented by multi-carrier modulations, where it was reported in [5] that the *"OFDM principle"*, with each data packet made up of a number of complex-valued sinusoids that are modulated by information symbols, still represents the leading concept of waveform design in future 5G communications exploiting mm-wave frequencies.

The achievements of [4] suggest that MIMO-based E-band connections could be profitably exploited for wireless backhaul of urban cells. For many years, cell backhaul has been exclusively managed by wired PSTNs and fiber links. However, with the progressive cell size reduction and the consequential increase of cells number, backhaul solutions had to become more cost effective, scalable and easy to install as compare to traditional macro backhaul technologies. Well-known wired technologies do not seem to cope with such soaring requirements and hence 3GPP standardization committee proposed wireless solutions for small cell backhauling, which are based on LOS/NLOS microwave connections and LOS mm-wave connections [6]. The importance of wireless backhaul will increase significantly in 5G, where the cell size is expected to reduce further. Authors of [7] claim that in 5G ultra-dense networks, the macrocell Base Station (BS) is configured only to transmit the management data for controlling the user handover in small cells and the small cell BS takes charge of the user data transmission. Therefore, the small cell network is not a complement for the macrocell network and hence it should be provided by autonomous backhauling capabilities that only dedicated wireless connections can fulfil.

Some past contributions preliminarily assessed the viability of mm-wave short-range connections, mainly in local networking applications. In [8], Dyadyuk *et. al.* developed a practical solution for LOS-based multi-gigabit point-to-point E-band transmission in the 81-86 GHz bandwidth. Such a solution is based on analogue Frequency Division Multiplexing (FDM) of the data stream, using root-raised cosine bandpass filters to shape the sub-channels. Additionally, [9] can be regarded as an improvement of [8], where the same FDM-based solution of [8] was used in conjunction with MIMO Spatial Multiplexing and Low-Density-Parity Check (LDPC) coding to boost the capacity of short-range point-to-point mm-wave LOS connections. Vertical-Bell Laboratories Layered Space-Time (VBLAST) technique [10] for successive interference cancellation has been used in [9] to reduce the impact of ICI on the receiver's (Rx) performance.

One of the early contributions about mm-wave small cell backhaul has been published in [11], where the authors showed that under LOS assumption and using MIMO multiplexing together with adaptive modulation and coding, it is possible to reach up to 10 Gb/s of backhaul capacity. Some more recent works inserted mm-wave backhaul in the framework of 4G and 5G systems. Authors of [12] consider 2×2 MIMO with spatial multiplexing for 28 GHz small-cell backhaul in 4G standards, where convolutional coded single-carrier M-ary QAM modulation has been used to transmit backhaul data. LOS-MIMO mm-wave backhaul exploiting Spatial Multiplexing was proposed in [13], where an array of 1m $\times$ 1m is used at the transmitter and receiver sides. Additionally, in order to improve the system's performance, while reducing baseband receiver complexity, Time-Hopping Impulse-Radio (TH-IR) transmission has been adopted in [14] for 81 GHz small-cell backhaul. In this work, single antenna system has been considered along with the hypothesis of *"pencil-beam"* LOS propagation. Furthermore, the work reported in [15] and [16] aims at integrating small-cell backhaul in the framework of massive MIMO systems, which is expected to be one of the key technologies of 5G and will make easier backhaul in large-scale and ultra-dense networks.

In this paper, we propose a practical system solution for small cell backhaul at mm-wave frequencies, based on MIMO and OFDM. The proposed solution relies on the use of Space-Time Shift Keying (STSK) in combination with maximum likelihood (ML) detection performed in the frequency domain. STSK is a space-time coding technique proposed to exploit the benefits of MIMO without the need for high-complexity detection algorithms [17]. STSK is a generalized shift-keying architecture utilizing both the space and time dimensions that is based on activation of indexed $Q > 1$ orthogonal space-time dispersion matrices within one symbol block duration. Due to such degrees of freedom, STSK is capable of striking a flexible diversity versus multiplexing gain trade-off, which is achieved by optimizing both the number and size of the dispersion matrices as well as the number of transmit and receive antennas. STSK can be regarded as an improvement of state-of-the-art MIMO multiplexing techniques, namely the Spatial Multiplexing (SMUX) and the Spatial Modulation (SM) [18]. SMUX, adopted by the largest

part of state-of-the-art contributions dealing with small cell backhaul, multiplexes a number of symbols in space domain such that the different symbol streams overlap over the MIMO channel. As a result, inter-channel interference (ICI) arises and must be dealt with at the receiver side using computationally intensive processing that becomes prohibitive for high number of antennas N. On the other hand, SM has been proposed in order to exploit the benefits of MIMO multiplexing, while reducing the required receiver complexity. SM activates only one transmit antenna for each symbol period, while the other $N - 1$ antennas remain silent. Therefore, in SM the ICI is avoided and optimum symbol detection can be implemented with affordable computational complexity. However, the multiplexing gain of SM is dramatically reduced with respect to SMUX. A simplified version of SM is Space-Shift Keying (SSK), which was proposed in [19] for E-band LOS backhaul applications. In SSK, the i-th symbol is univocally individuated by the i-th activated antenna. Despite the reduced complexity of the detection and favourable BER performance achieved, SSK fails to provide an acceptable throughput when small-size MIMOs are used. On the other hand, STSK has the capability to increase the multiplexing gain by increasing the number of dispersion matrices without increasing the number of antennas.

The advantages of STSK make it suitable for future multi-gigabit mm-wave communications, in particular when small cell backhaul in dense urban scenarios is considered. Indeed, the mm-wave propagation in dense urban environment actually presents some challenging aspects, where it was shown in [4] that besides LOS and NLOS the mm-wave channel exhibits a third *outage* state, where signal-to-noise ratio (SNR) at the receiver is approaching $-\infty$ dB. This is due to the fact the path loss, in either LOS or NLOS state, is sufficiently large to drop the SNR below any acceptable threshold. In [4] a three-state probabilistic channel model is proposed in order to take into account the outage situation. Such a model is based on the computation of LOS, NLOS and outage probabilities, which substantially depends on the transmitter's and receiver's antenna distance and the surrounding environment. On the basis of this model, the probability of NLOS channel state significantly increases with the antenna distance. Under these critical propagation conditions, the available power resources may be severely limited and robust transmission solutions should be envisaged.

Small-cell backhaul application is particularly critical, where it is characterized by stringent requirements in terms of low bit-error-rate ($\leq 10^{-6}$) and high availability (possibly 99.999% or "*five 9s*"). Therefore, transmission robustness is the first issue to be addressed followed by throughput analysis, because the data rate of backhaul network should be high enough to convey information with minimum latency. Therefore, in this paper we consider STSK-OFDM as a valuable solution to support mm-wave small-cell backhaul in highly-critical and potentially-hostile metropolitan scenarios.

The common factor of most of related state-of-the-art contributions is the assumption of *free-space* LOS propagation

regarded as necessary condition in order to guarantee backhaul connectivity, while different propagation modalities are generally assumed as "*outage*". However, the presence of free-space LOS between base stations cannot be realistically assumed by default in small cell urban scenarios. In such a framework, STSK can offer an efficient trade-off between MIMO diversity and multiplexing, allowing to configure the backhaul system in a way to improve link performance, while also achieving a satisfactory data throughput.

The rest of the paper is structured as follows. Section II will consider requirements and constraints of mm-wave small cell backhaul, Section III covers the mm-wave MIMO-STSK backhaul system with OFDM transmission. Section IV analyzes the mm-wave channel in the urban scenarios considered for small-cell backhaul. Section V discusses selected simulation results in terms of link performance and coverage. Finally, conclusions are drawn in Section VI.

II. REQUIREMENTS AND CONSTRAINTS OF SMALL-CELL WIRELESS BACKHAUL

Traffic generated inside a cell is transported to the core network using the backhaul and hence the availability of the backhaul links is essential to guarantee the required throughput inside a cell. Some essential requirements on small-cell backhaul are listed as follows [20]:

- To support the traffic originated in each cell on the scale of hundreds of Mbps;
- To support NLOS connections;
- To connect tens of small cells in an area of few kilometers, assuming that small cells are deployed with spacing 30 to 300 m;
- To minimize the latency up-to sub-millisecond.

Unlike access, continuous link availability is essential for backhaul. For example 4G/LTE-A requirements point out very high link availability of "*five 9s*" at BER less than or, at most, equal to 10^{-6} [21]. Such a claim is contradicted by the application note of Ceragon corp. (Palo Alto, CA) [22], where it is stated that "*five 9s*" availability is not strictly required for small-cell backhaul. Their motivation is that small cells form an offload underlay to a higher-availability macrocell. The exploitation of E-band frequencies for small-cell backhaul would allow in principle to cope with the broadband connectivity requirements listed above. The use of robust MIMO space-time coded transmission should enhance link availability and coverage under critical NLOS propagation conditions typical of 5G urban scenarios.

In Fig. 1 we depict the dense-urban backhaul scenario considered in our work, where some small transceiver base stations offering connectivity to small-cell users are mounted on street poles. The height of street poles in US is 8 meters, so it is reasonable to suppose that BS equipment is placed 6-7 meters from the ground level. On the other hand, the "*macro BS*" representing the main node of the backhaul network is placed on the rooftop of a tall building of 20 meters height. Fixed and mobile potential obstructions due to buildings and other elements are present between transmit and
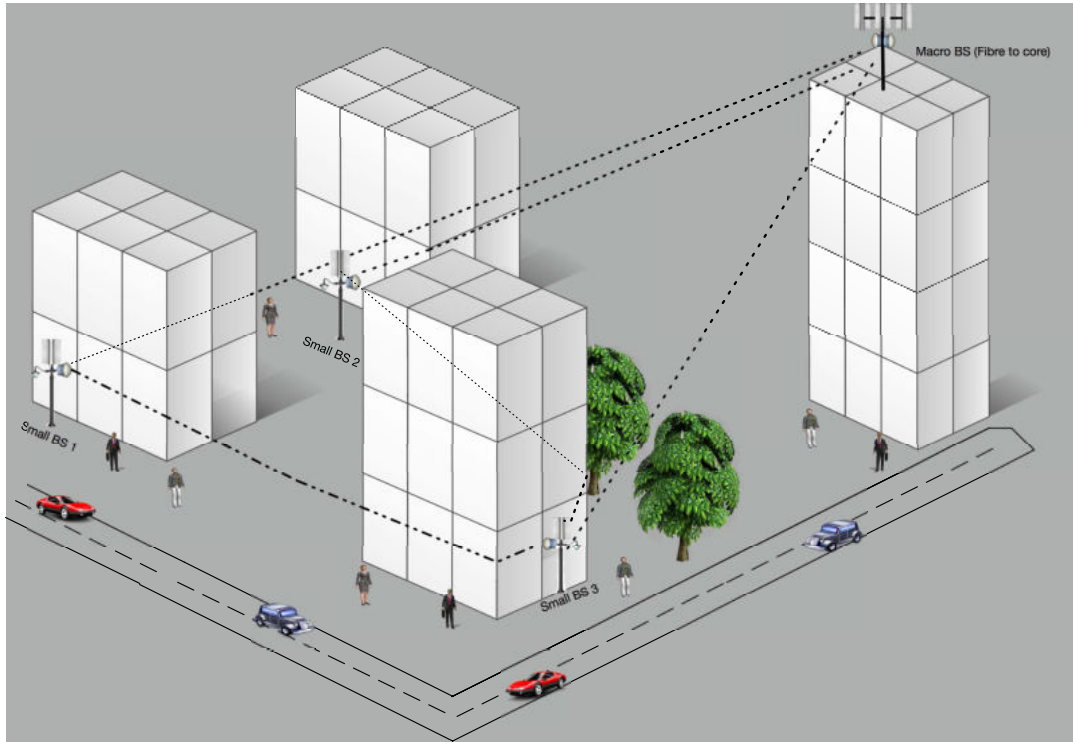
FIGURE 1. Small cell backhaul in dense urban environment.

receive antennas, which would affect the propagation characteristics such that the presence of LOS backhaul cannot be guaranteed a priori. Moreover, for long distances, the outage occurrence should also be considered. For these reasons, the three-state channel modelling proposed in [4] are considered appropriate to describe large scale and small scale propagation impairments characterising the scenario drawn in Fig. 1. In Section IV, the detailed channel modelling concerning the considered backhaul application will be provided.

III. STSK MIMO-OFDM SYSTEM FOR MM-WAVE SMALL-CELL BACKHAUL
A. INTRODUCTION TO STSK AND COMPARISON WITH OTHER SPACE-TIME CODING TECHNIQUES
Space-Time Shift Keying (STSK) technique is a generalized shift-keying architecture utilizing both the space and time dimensions. STSK is based on the activation of one of Q appropriately indexed space-time dispersion matrices within each STSK block duration T_B. In STSK $log_2(Q)$ bits index a dispersion matrix selected from among Q available dispersion matrices of size $N \times T$, where N is the number of transmit antennas and $T \leq N$ is the number of columns of the dispersion matrix. The selected dispersion matrix disperses the energy of the input information symbol taken from an L-ary PSK or QAM constellation, which is indexed by the remaining bits of the transmitted block [23]. The STSK transmitted signal can be expressed as follows [23]:

$$X_{STSK}(i) = S_1(i) \times \mathbf{0}_{N \times T} + \cdots + S_q(i) \times \mathbf{A_q}(i)$$
$$+ \cdots + S_Q(i) \times \mathbf{0}_{N \times T} \qquad (1)$$

where $S_q(i)$ is the transmitted complex symbol and $\mathbf{A_q}(i)$ is the selected dispersion matrix, which can be represented as:

$$\mathbf{A_q}(i) = \begin{bmatrix} a_1^1 & \cdots & a_1^T \\ \vdots & \ddots & \vdots \\ a_N^1 & \cdots & a_N^T \end{bmatrix} \in \mathbb{C}^{N \times T} \qquad (2)$$

The zero matrices in (1) are related to the de-activated dispersion matrices, where only one matrix q is activated during each symbol transmission [23]. Every column of the selected matrix is then transmitted from N-antenna array at a baud-rate T/T_B.

Four parameters characterize STSK transmission, including the number of transmit antennas N, the number of receive antennas M (in a backhaul system $N=M$), the cardinality of the set of dispersion matrices Q and T. Hence, in the following discourse the specific STSK configurations will be identified by a vector of parameters *(N,M,T,Q)*.

The computation of the dispersion matrices has been performed off-line, by following the criterion shown in [24]. Substantially, the pairwise error probability of STSK has been minimized by means of a near-optimal and computationally tractable Genetic Algorithm, applied to a population made of dispersion matrix sets.[1]

STSK can be regarded as an extension and improvement of SM [23]. More specifically, SM can be regarded as a special case of STSK by imposing T=1 and

$$\mathbf{A_q^{SM}}(i) = \begin{bmatrix} 0 & \cdots & 1 & \cdots & 0 \end{bmatrix}' \in \mathbb{R}^{N \times 1} \qquad (3)$$

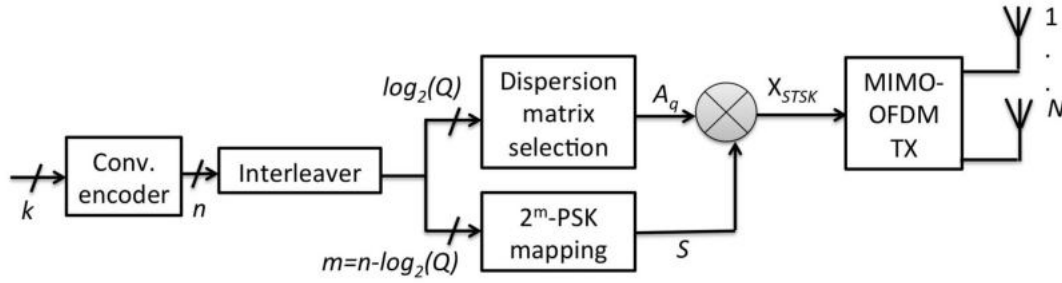[1] Please refer to [24] for further details.

FIGURE 2. Convolutionally-encoded STSK (CESTSK) transmission scheme for mm-wave backhaul.
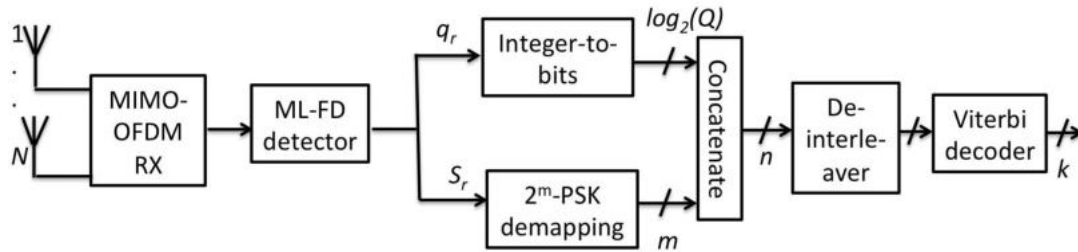

FIGURE 3. Convolutionally-encoded STSK (CESTSK) receiver scheme for mm-wave backhaul.

where the non-zero element is in the position q of the array. For completeness and for the sake of comparison, the SMUX transmitted symbols vector can be expressed in the following manner:

$$\underline{X}_{SMUX} = \mathbb{I}_N \underline{S}(i) \qquad (4)$$

where $\mathbb{I}_N$ is identity matrix and $\underline{S}(i)$ represents the transmission vector of size $N \times 1$. It is interesting to note that the throughput of STSK does not depend on the number of transmit antennas N, as shown in (5). The STSK throughput can be increased by: i) increasing the modulation order L, ii) increasing the number of dispersion matrices Q and iii) decreasing the dispersion matrix duration T. Increasing Q may increase the pairwise error probability as reported in [17], where it was suggested that $Q = 4$ is a satisfactory tradeoff between efficiency and performance. Thus, it is better to tune the modulation order L and T in order to efficiently manage the trade-off between diversity and multiplexing.

$$\eta(STSK) = \frac{log_2(L) + log_2(Q)}{T} \; [b/s/Hz] \qquad (5)$$

Furthermore, the throughput of SM logarithmically increases with the number of transmit antennas, as shown in (6), while the throughput of SMUX increases linearly with N, as shown in (7).

$$\eta(SM) = log_2(L) + log_2(N) \; [b/s/Hz] \qquad (6)$$

$$\eta(SMUX) = N log_2(L) \; [b/s/Hz] \qquad (7)$$

As correctly stated in [23], the augmented diversity of STSK, achieved both at the transmitter and receiver side, comes at the price of potential decrease of throughput with

respect to SM that exploits receive diversity only. When compared with SMUX, both STSK and SM achieve lower throughput. However, it should be highlighted that SMUX does not provide any diversity gain against multipath effects, offering multiplexing gain only equal to the number of transmit antennas. STSK is more flexible than SMUX as it can tune different parameters to achieve a trade-off between diversity and multiplexing, while in SM higher throughput can be obtained only by exponentially increasing the number of transmit antennas with a considerable increase of hardware costs.

B. DESCRIPTION OF THE mm-WAVE STSK-BASED MIMO-OFDM TRANSCEIVER FOR SMALL CELL BACKHAUL

In this paper, we propose to evaluate two MIMO-OFDM STSK schemes, which differ in the way the channel coding is applied to the transmitted bit stream. The first scheme is referred to as *convolutionally-encoded STSK (CESTSK)*, which is shown in Fig. 2. In the CESTSK scheme, the set of n bits forming the transmitted block are taken from the interleaved output of a convolutional encoder at rate k/n. Therefore, both the $log_2(Q)$ bits selecting the dispersion matrix and the remaining m bits indexing the 2^m-ary PSK symbol are encoded and interleaved. The convolutionally-encoded STSK matrix columns are then transmitted over P OFDM subcarriers. The corresponding receiver scheme is shown on Fig. 3.

The second scheme is referred to as *Trellis-coded STSK (TCSTSK)*, whose transmitter block diagram is shown in Fig. 4 and the receiver structure is shown in Fig. 5.
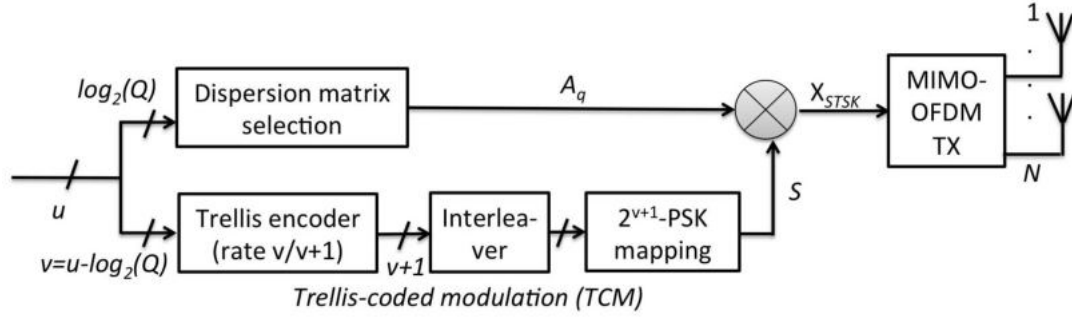
FIGURE 4. Trellis-encoded STSK (TCSTSK) transmission scheme for mm-wave backhaul.
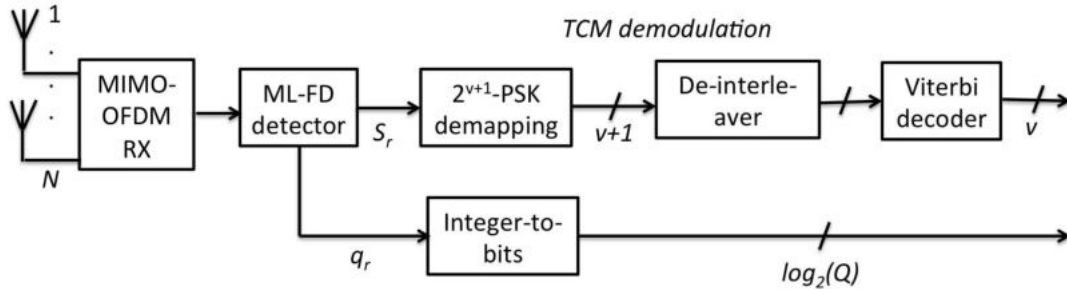

FIGURE 5. Trellis-encoded STSK (TCSTSK) receiver scheme for mm-wave backhaul.

The TCSTSK has been derived by the TCM approach for SM (TCSM) considered by Mesleh *et. al* in [25]. In this scheme, the $log_2(Q)$ bits selecting the dispersion matrix are uncoded, while the remaining v bits of the block produce a TCM symbol, which is multiplied by the dispersion matrix. The CESTSK scheme is more robust against noise and channel effects, while the TCSTSK scheme gains in terms of throughput efficiency. More precisely, the normalized throughput offered by the two schemes is given as follows:

$$\eta\,(CESTSK) = \frac{k(m + log_2\,(Q))}{nT}\,[b/s/Hz] \qquad (8)$$

$$\eta\,(TCSTSK) = \frac{v + log_2\,(Q)}{T}\,[b/s/Hz] \qquad (9)$$

Both schemes rely on maximum-likelihood detection performed in the frequency domain (ML-FD). One of the main advantages of OFDM-MIMO systems is the possibility of applying the optimum ML detection at the subcarrier level with tolerable computational complexity [23]. Indeed, ISI-free OFDM transmission with cyclic prefix converts a frequency-selective fading channel into P statistically-independent flat-fading channels. Hence in our OFDM-STSK schemes, FD-ML finds the optimum vector (q_{opt}, k_{opt}) miminizing the following metric [23], where the index i is related to the current signaling period:

$$\left(q_{opt}, k_{opt}\right) = \min_{q,k}\left\{\left\|\mathbf{Y_p}\,(\mathbf{i}) - \mathbf{H_p}\mathbf{C}\underline{\kappa}_{q,k}\,(i)\right\|^2\right\},$$
$$p = 0, \cdots, P - 1 \qquad (10)$$

where:

- $\mathbf{Y_p}\,(\mathbf{i}) \in \mathbb{C}^{NT \times 1}$ is the vectorial stacking of the MIMO-STSK signal received over the pth subcarrier;
- $\mathbf{H_p} \in \mathbb{C}^{NT \times NT}$ is the channel matrix related to the pth subcarrier;
- $\mathbf{C} = \left[vec\,(A_1)\,, \cdots, vec\,(A_Q)\right] \in \mathbb{C}^{NT \times Q}$, with $vec()$ being the vectorial stacking operator;
- $\underline{\kappa}_{q,k}\,(i) = \left[\underbrace{0, \cdots, 0}_{q-1}, \hat{S}_k, \underbrace{0, \cdots, 0}_{Q-q}\right]$, where $\hat{S}_k$ is one of the symbol belonging to the PSK constellation.

Finally, given the optimum estimation of the dispersion matrix index (q) and of the encoded transmitted PSK-symbol S_k, the information bit block is finally decoded, as shown in Fig. 3 and 5.

IV. mm-WAVE BACKHAUL CHANNEL MODELING AND LINK IMPAIRMENTS

In this section, the mm-wave backhaul channel modeling will be considered in details, together with the most significant link impairments affecting the system performance.

A. SMALL-SCALE PROPAGATION PHENOMENA: MULTIPATH FADING

MIMO channel capacity is severely limited by transmit and receive spatial correlations [26]. As discussed in [27], the mm-wave MIMO channel can be modelled using time

clusters and spatial lobes. Hence, the statistical spatial channel model (SSCM) used in this work is based on temporal clusters and spatial lobes, as described in [28]. It is proven in [29] that power delay profiles (PDP) at mmWave frequencies are obtained with greater temporal resolution on the order of 2.5 ns and also narrower spatial resolutions on the order of 7° to 10° compared to the channel models for sub-10GHz. This actually shows that temporal clusters are composed of many intra-cluster sub-paths with different random delays as described in [27].

The MIMO channel impulse response [28] can be modelled using a double-directional time invariant model represented as:

$$h\left(t, \vec{\theta}, \vec{\Phi}\right) = \sum_{s=1}^{S} \rho_s e^{(j\varphi_s)} \delta(t - \tau_s) \delta\left(\vec{\theta} - \vec{\theta}_s\right) \delta\left(\vec{\Phi} - \vec{\Phi}_s\right) \tag{11}$$

where

- S is the total number of multipath components;
- t is the propagation time;
- ρ_s is the amplitude of s-th multipath component;
- φ_s and τ_s are phases and propagation time delays of s-th multipath component, respectively;
- $\vec{\theta}_s, \vec{\Phi}_s$ is the vector containing the azimuth/elevation Angle-of-Direction (AoD) and Angle-of-Arrival (AoA) for the s-th multipath component, respectively.

The non-parametric omnidirectional MIMO channel for the s-th multipath component is given by [28]

$$\mathbf{H}_s = \mathbf{R_r}^{1/2} \mathbf{H}_w \mathbf{R_t}^{1/2} \tag{12}$$

where $\mathbf{H}_s$ is $N \times M$ MIMO channel matrix, $\mathbf{R_r}$ and $\mathbf{R_t}$ represent the receive and transmit spatial correlation matrices, respectively. The transmit and receive MIMO correlation between two antenna elements (n, m) for uniform linear array (ULA) configuration as given in [28] as

$$\mathbf{R^{n,m}} = \left(\mathbf{A}e^{-\mathbf{B} \cdot \zeta_{n,m} \cdot \lambda \cdot \mathbf{d_{n,m}}} - \mathbf{C}\right) e^{-\mathbf{j} \cdot \mathbf{U}(-\pi, \pi) \cdot \mathbf{d_{n,m}}} \tag{13}$$

where $\mathbf{A}$, $\mathbf{B}$ and $\mathbf{C}$ are spatial correlation coefficients depending on the channel environment conditions such as LOS or NLOS, $\zeta_{n,m}$ represents the spacing between adjacent Tx or Rx antenna elements in units of wavelengths, λ is the carrier wavelength, $d_{n,m}$ is the absolute distance between adjacent Tx or Rx antenna elements, and $U(-\pi, \pi)$ is the uniform random variable generated in the range $-\pi$ and π. $\mathbf{H}_w$ matrix entries correspond to small scale spatial path amplitudes and phases as in (11) without considering the parametric components, whereas the entries of $\mathbf{R_r}$ and $\mathbf{R_t}$ are related to parametric components including AOD, AOA and angular spread of the transmitter and receiver. $\mathbf{H}_y$ retains the characteristics of the autocorrelation of the multipath components specified by the spatial correlation matrices as in (12), while retaining the small scale distribution specified in $\mathbf{H}_w$ (Rician in case of LOS and Rayleigh in case of NLOS). Unlike current channel models that use global azimuth and elevation spreads to

quantify the degree of angular dispersion, RMS lobe angular spread [27] is considered in this work that is different from global angular spread, because only the strongest measured lobe directions are assumed in case of RMS lobe angular spread.

B. LARGE-SCALE PROPAGATION PHENOMENA: PATHLOSS, GASEOUS ABSORPTION AND RAIN ATTENUATION

In the design of mm-wave transmission systems, the impact on link budget of large-scale propagation phenomena should be carefully assessed. Indeed, pathloss and atmospheric attenuations affecting mm-wave bands are much larger than those measured in sub-6 GHz bands. The comprehensive link attenuation due to large scale propagation, denoted by L_{bh}, can be expressed as follows:

$$L_{bh} = PL + L_{O_2} + L_{rain} + \epsilon_s \ (dB), \tag{14}$$

where PL represents the pathloss, L_{O_2} represents the oxygen absorption, L_{rain} denotes the rain attenuation and ϵ_s is the shadowing contribution, modeled using a Gaussian random variable with zero mean and standard deviation depending on the specific propagation environment [30].

TABLE 1. Large-scale link attenuations in mm-wave backhaul: modeling and parameterisation.

	Analytical Expression	Parameters (@73 GHz)
PL	$\alpha + \beta 10 log_{10}(d_{m.})$	α_{NLOS}=86.6 β_{NLOS}=2.45 α_{LOS}=69.2 β_{LOS}=2
L_{rain}	$\mu\{F(p_{rain})\}^{\xi} d_{km.}$	μ=1.0764 ξ=0.7268
L_{O_2}	$K_{O_2} d_{km.}$	K_{O_2}=0.3

In Table 1, analytical modeling and parametrization of large-scale backhaul link attenuations versus distance d are conveniently summarized, where the model and numerical parameters for pathloss have been taken from [4]. As far as rain attenuation is concerned, the simple and effective Crane model [31], also adopted by the International Telecommunication Union (ITU), has been considered. The parameter $F(p_{rain})$ represents the rainfall intensity in mm/h, given as function of the probability p_{rain} that the rain fall intensity F is not exceeded. The mapping of p_{rain} versus F is derived by experimental meteorological data. Finally, the oxygen absorption has been considered using the experimental curves shown by the FCC report of [32].

C. THREE-STATE CHANNEL MODEL
In [4], the probabilistic analyses with respect to the backhaul distance (d) for the three-state channel model are represented as follows:

$$P_{outage}(d) = max\{0, 1 - exp(-a_{out}d + b_{out})\} \tag{15}$$

$$P_{LOS}(d) = \{1 - P_{outage}(d)\} exp(-a_{LOS}d) \tag{16}$$

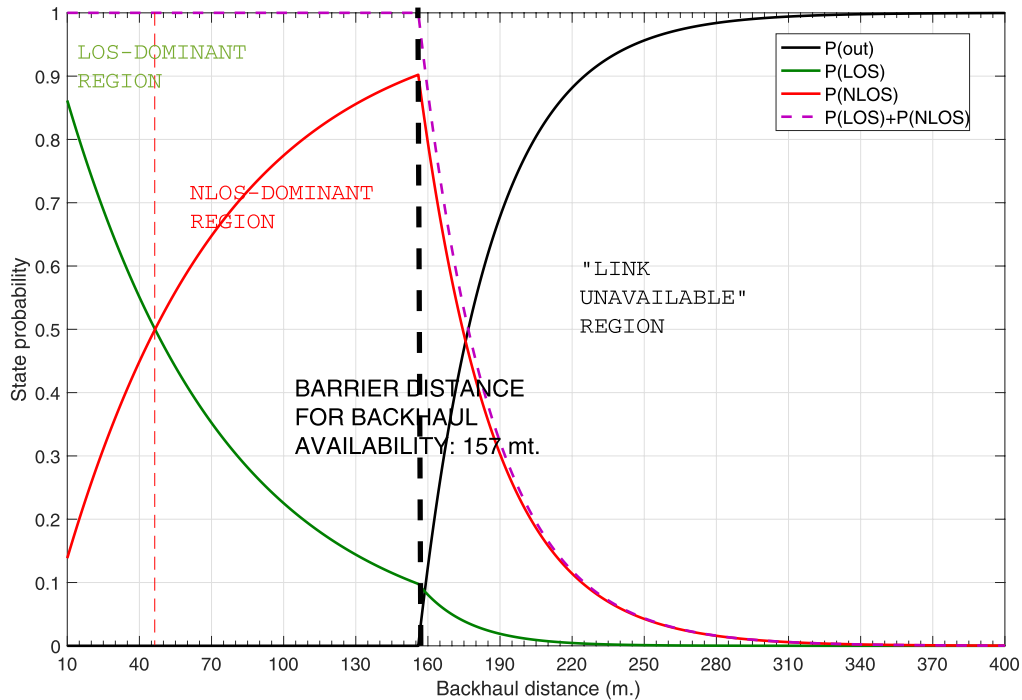$$P_{NLOS}(d) = 1 - P_{LOS}(d) - P_{outage}(d) \tag{17}$$

FIGURE 6. Three-state channel probabilities vs. backhaul distance.

The parameters used in (15)-(17) have been derived in empirical manner from the NYC measurement campaign, where $1/a_{LOS} = 67.1$ m., $1/a_{out} = 30.0$ m. and $b_{out} = 5.2$. Authors of [4] warmly suggest caution in generalizing these particular parameters in other scenarios, where the outage probability is strictly dependent on the communications environment. However, we think that the three-state assumption will lead to a more accurate and realistic analysis of the backhaul performance in terms of coverage.

Fig. 6 shows the three probability functions versus *d*, where three propagation regions can be identified, which include a "*LOS-dominant*" region, whose distance limit is around 46 m., a "*NLOS dominant*" region extended until 155-160m. Then, increasing the distance beyond 160m, we access the outage region, where the backhaul link is most likely to be unavailable. Indeed, in the outage state, the pathloss is likely to be infinite and hence the destination signal-to-noise ratio is severely degraded. The definition of "*small cells*" claims that the maximum cell diameter is 200 meters, which exceeds the barrier distance for backhaul link availability shown in Fig. 6 and for this reason it should be regarded as an upper bound on the reachable coverage.

D. NON-IDEAL BEHAVIOR OF RF HARDWARE

As the considered small-cell backhaul transmission system is based on MIMO and multi-carrier modulation, we should take into account the non-ideal behavior of Radio Frequency (RF) hardware, in particular power amplifiers and mm-wave oscillators.

Terrestrial mm-wave power amplifiers are based on solid-state technology, which generally produce severe amplitude distortion due to saturation of amplitude-to-amplitude (AM/AM) characteristic, but negligible phase drifts. If the amplifier is driven in saturation by an OFDM signal, then amplitude clipping results in non-linear distortion of the received waveform [33]. The easiest and most used way to counteract the effects of non-linear amplification is to drive back the amplifier characteristic to the linear zone, thus introducing an input backoff (IBO). The resulting output backoff (OBO) will decrease the power efficiency of the transmission system. Hence, IBO/OBO is considered in this work to avoid non-linear effects with the aim that in future we shall be discussing the analysis of appropriate countermeasures in MIMO-OFDM transceivers against non-linear distortions or, as alternative, the adoption of waveforms less prone to amplifier non-linearity.

High-frequency oscillators are generally affected by frequency drifts due hardware imperfections, which is known as *phase-noise*. The impact of phase noise on MIMO-OFDM transmission systems has been thoroughly investigated by Rao and Daneshrad in [34]. Substantially, phase-noise produces two contributions affecting the output of the OFDM receiver related to each antenna element: a constant phase-error (CPE) term that is common to all subcarriers and an additional ICI term that is due to the sum of the skirts of the phase-noise spectrum from the neighboring subcarriers in an OFDM block. The CPE term does not impact a lot on MIMO-OFDM performance, as clearly demonstrated in [34]. The ICI term is more destructive, as it depends on the

TABLE 2. 2×2 MIMO transmission configurations.

2x2 MIMO					
	Modulation	*Coding rate*	*Q*	*T*	*Net data throughput*
CESTSK	QPSK	0.5	4	2	1 b/s/Hz
TCSTSK	QPSK	0.5	4	2	1.5 b/s/Hz
CESM	BPSK	0.5	N.A.	N.A.	1 b/s/Hz
TCSM	QPSK	0.5	N.A.	N.A.	2 b/s/Hz
CE (TC) SMUX	QPSK	0.5	N.A.	N.A.	2 b/s/Hz

TABLE 3. 4×4 MIMO transmission configurations

4x4 MIMO					
	Modulation	*Coding rate*	*Q*	*T*	*Net data throughput*
CESTSK	QPSK	0.5	4	2, 4	1 b/s/Hz, 0.5 b/s/Hz
TCSTSK	QPSK	0.5	4	2, 4	1.5 b/s/Hz, 0.75 b/s/Hz
CESM	QPSK	0.5	N.A.	N.A.	2 b/s/Hz
TCSM	QPSK	0.5	N.A.	N.A.	3 b/s/Hz
CE (TC) SMUX	QPSK	0.5	N.A.	N.A.	4 b/s/Hz

phase-noise PSD and on the codewords transmitted over the other subcarriers. It would be theoretically possible to deal with such a term with the maximum likelihood detection applied in the frequency domain, but the computational burden of the receiver scheme would become exponential with the subcarrier number. On the other hand, frequency error compensation techniques directly working in RF may increase the hardware complexity to a greater extent. Hence, in realistic small-cell backhaul applications, we should accept the presence of ICI term with potentially-detrimental effects. Indeed, MIMO decoding allows at averaging all channel effects, including phase-noise, as shown in [34]. We might expect that keeping phase noise conveniently low and considering the presence in the transmission chain of convolutional coding and interleaving, no error-floor due to the ICI term will be noticed.

V. SIMULATION RESULTS: LINK PERFORMANCE AND COVERAGE
A. SIMULATION STRATEGY AND CONFIGURATION SETUP
In order to evaluate the proposed MIMO-STSK system for mm-wave small-cell backhaul, intensive simulation has been performed in MATLAB environment. The results provided by STSK will be compared with those of state-of-the-art SM and SMUX techniques, already considered in the literature for backhaul transmission. The simulation approach is motivated by the impossibility of dealing with closed-form analytical error probability expressions for the mm-wave

channel scenario, while accounting for both propagation and RF hardware impairments. Two different series of results will be presented in this section:
- *Link performance results*, in terms of bit-error-rate (BER) versus per-bit AWGN signal-to-noise ratio E_b/N_0. These results show the behavior of CESTSK and TCSTSK schemes against the considered counterparts in the presence of small-scale propagation (NLOS and LOS) and phase noise;
- *Coverage results*, in terms of maximum backhaul distance for which the target BER of 10^{-6} is obtained for different availability rates, namely 99.999%, 99.99% and 99.9%.

In Table 2 and 3, the different MIMO transmission configurations considered in our simulations have been detailed in terms of modulation format, channel coding rate and STSK parametrization. The convolutional coding rate has been fixed to 1/2 and random interleaving has been adopted. The selected modulation format is the QPSK, apart for CESM, where the combination 1/2-trellis coding and QPSK is not applicable, where in this case BPSK modulation was considered. The net data throughput achieved by the different MIMO techniques is shown in the last column of Table 2 and 3.

As already evidenced, STSK throughput does not depend on the number of Tx/Rx antennas and is lower or at most equal to that of SM. In all cases, trellis-coded MIMO transmission provide an increase of spectral efficiency of 30-50% more than convolutionally-encoded transmissions.
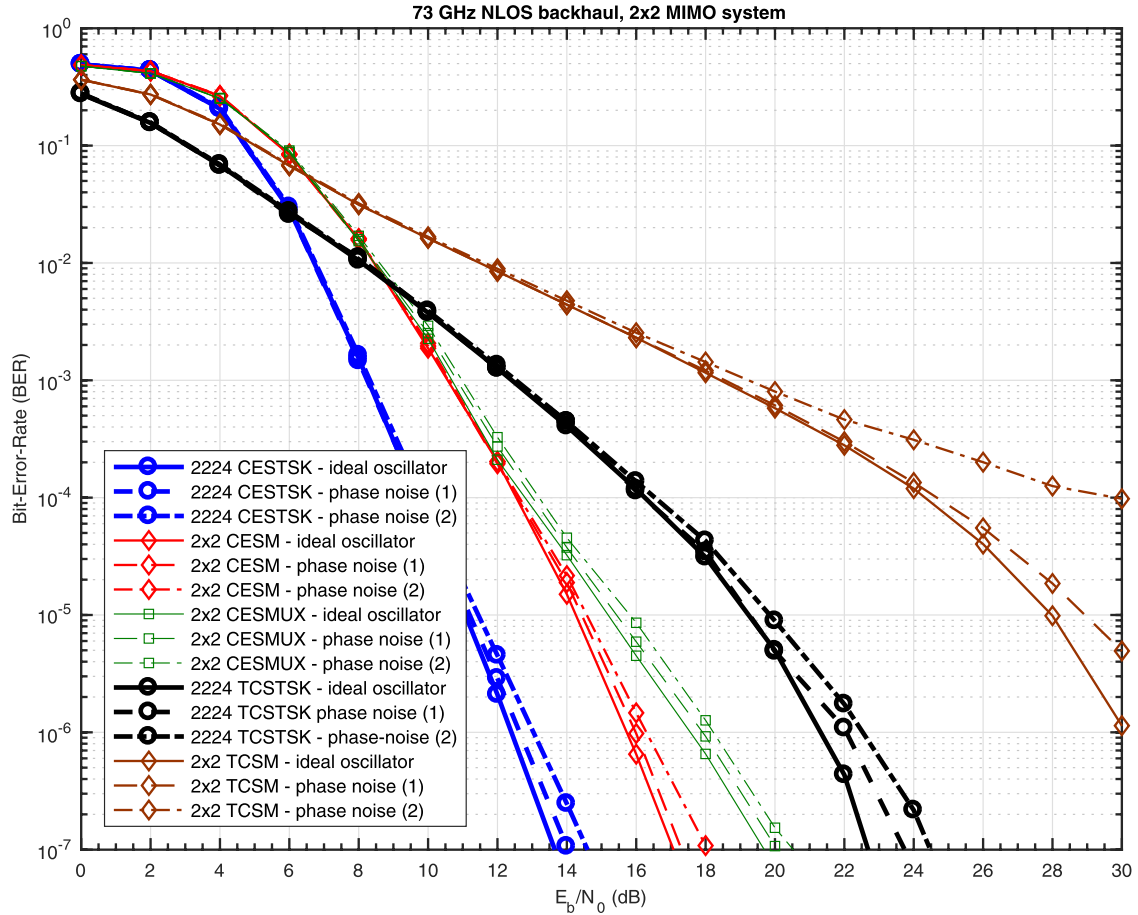
FIGURE 7. BER vs.E_b/N_0 for 2x2 MIMO small-cell backhaul system: NLOS channel state.

Finally, it should be noticed that trellis-coded and convolutionally-encoded transmission are exactly the same for SMUX, because neither antenna nor dispersion matrix selection is performed.

As far as OFDM transmission is concerned, the number of subcarriers P has been fixed to 512 and the cyclic prefix length to 200 symbols in order to cope with the channel impulse response length. Optimum maximum likelihood detection, applied in the frequency domain (FD-ML), is considered for all MIMO-OFDM transmission modalities (FD-ML for SM and SMUX is detailed in [18] and [35] respectively), under the hypothesis of ideal knowledge of channel state information (CSI). The impact of CSI estimation errors on STSK link performance will be matter for future work. Finally, the amount of bandwidth used for backhaul transmission consists of a 500 MHz slot allocated in the 73 GHz E-band portion.

B. LINK PERFORMANCE ANALYSIS

First we consider the link performance for a 2×2 MIMO backhaul system, which are shown in Fig. 7 and 8. In these simulations, the clustered multipath has been modeled as

described in Section IV-A, while the phase noise PSD has been parametrized using the two masks of [36] and [37] labelled in the inner captions of the figures as phase-noise(1) and phase-noise(2), respectively. The first oscillator is a low-noise SiGe component, part of an RF chip-set for the E-band mobile backhaul application, while the second oscillator is a Voltage Controlled Oscillator (VCO) used to implement a Phase-Locked-Loop (PLL) for coherent detection of L-QAM signals, which is tunable in the frequency range from 70.5 to 85.5 GHz. The numerical values in dBc/Hz of the two phase-noise PSDs at the frequencies of 1 MHz and 10 MHz are reported in Table 4.

TABLE 4. Phase noise masks of the considered E-band oscillators (values in dBc/Hz).

	phase-noise (1) [36]	phase-noise (2) [37]
1 MHz	-105	-97.73
10 MHz	-125	-116.79

As shown in Fig.7 and 8, the performance improvement attained by CESTSK compared to CESM and CESMUX is evident at a glance. The impact of phase noise on the link performance looks very modest for both the
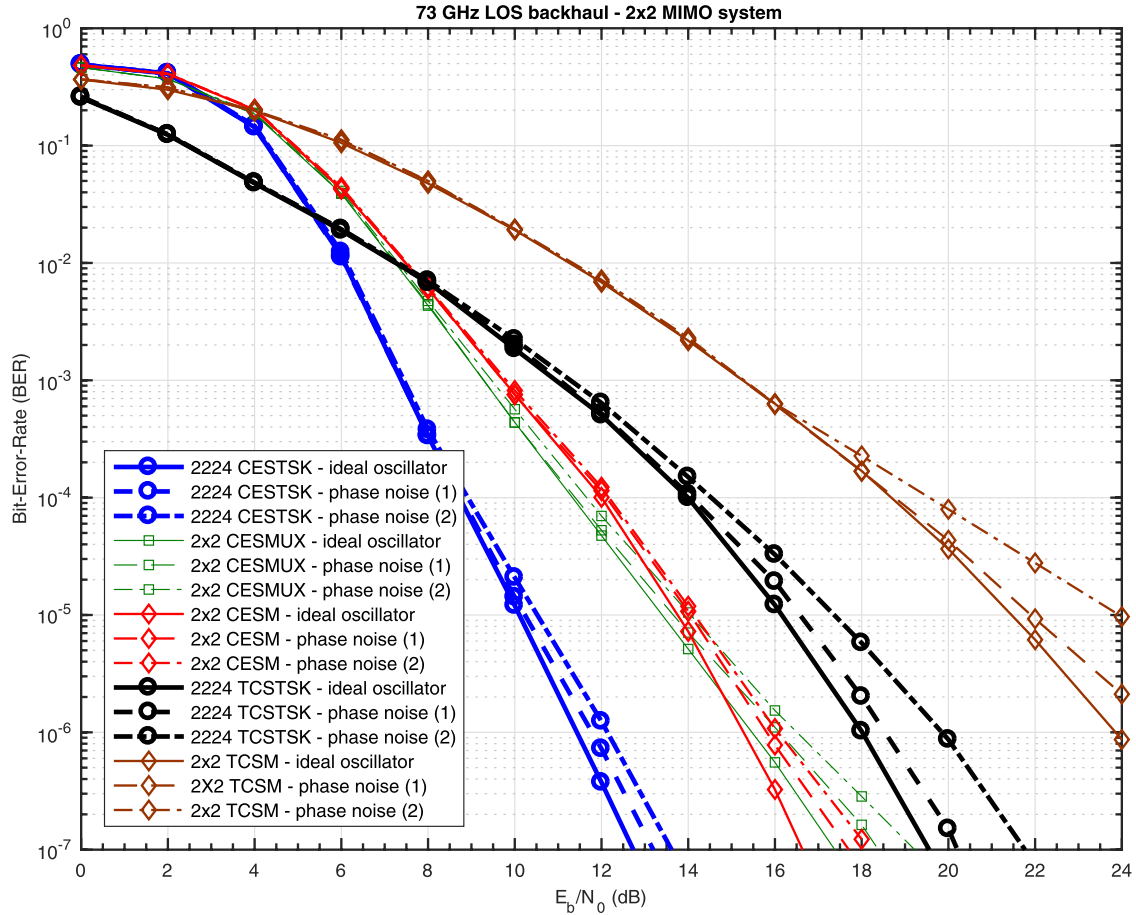
FIGURE 8. BER vs.E_b/N_0 for 2x2 MIMO small-cell backhaul system: LOS channel state.

considered oscillators. It is worth noting that CESM performs slightly better than CESMUX both in NLOS and LOS channels. This can be due to the receiver diversity attained by spatial modulation. On the other hand, when considering TCSTSK, we can notice a dramatically-decreased BER curve as compared to TCSM, in particular when the oscillator of [37] is employed. In general, trellis-coded STSK performs worse than convolutionally-encoded MIMO transmission techniques, because the correction capability of Viterbi decoding is not completely exploited, when the bits selecting the dispersion matrices are not encoded.

Additionally, the BER results for the 4×4 MIMO system are shown in Fig. 9 and Fig. 10, which fully confirm the trend observed for the 2×2 case, even fostering the improvement yielded by STSK. The flexibility inherent to STSK allows to consider two values for the parameter T, namely: $T = 2$ and $T = 4$, relaxing diversity and incrementing multiplexing in the first case and vice-versa in the second case. The $(4, 4, 2, 4)$ and $(4, 4, 4, 4)$ CESTSK dramatically outperforms the rest of the assessed techniques in both LOS and NLOS scenarios. It is also worth noting the dramatic performance improvement achieved by CESM and TCSM as compared

to lower diversity MIMOs as shown in Fig. 7 and Fig. 8. Indeed, as observed in literature, spatial modulation benefits a lot from receiver diversity, in particular when the multipath channel exhibits correlation.

In the 4×4 MIMO case, the phase noise impact on the BER performance is absolutely irrelevant for STSK, for both the CE and TC systems, and generally the impact of phase noise on the performance is reduced for all assessed techniques due to the averaging of jittering effects observed in [34].

C. COVERAGE ANALYSIS
The link performance shown in subsection V-B demonstrate the superiority of CESTSK (and partially of TCSTSK) compared to the SM and the SMUX techniques. This performance improvement is obtained at the price of a considerable reduction of the useful bit rate. In order to definitely assess the viability of the proposed technique for small-cell backhaul, the reachable coverage should be investigated by considering the operational requirements of BER and link availability typical of small-cell backhaul. Hence, in this section we consider the most stringent requirement of "*five 9s*" availability as baseline. This can be interpreted as having a target BER of
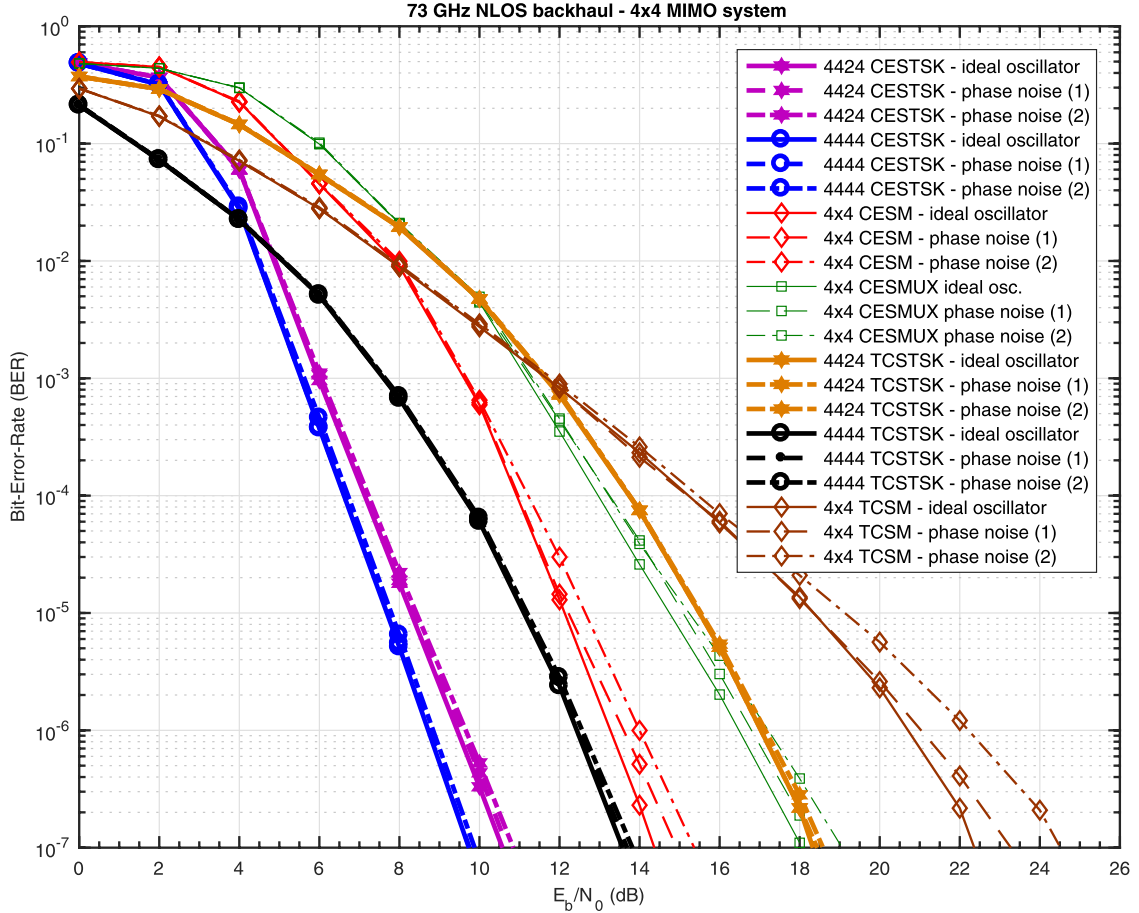
FIGURE 9. BER vs. E_b/N_0 for 4x4 MIMO small-cell backhaul system: NLOS channel state.

10^{-6} maintained for 99.999% of the operational time. Then, after having tested the coverage reachable by the different MIMO techniques under "*five 9s*" constraint, we relax the availability rate.

Define the "*out-of-service*" as the complementary event of "*link available*" and hence the out-of-service probability, denoted by γ, is accordingly computed. In this series of simulations, the average BER versus backhaul distance for a given out-of-service probability γ, is evaluated by applying the Bayes' theorem in the following manner:

$$P_b(d, \gamma) = P_{LOS}(d) P_{b/LOS}(d, \gamma)$$
$$+ P_{NLOS}(d) P_{b/NLOS}(d, \gamma) + 0.5 P_{outage}(d)$$
$$(18)$$

In our simulation we fix the outage probability P_{outage} to 0.5, while the other two conditional probability terms in (18) are obtained using the link simulations of Section V-B with the chosen channel state (LOS or NLOS) and setting the input signal-to-noise ratio with the value that is exceeded at distance d with probability equal to $(1 - \gamma)$. The signal-to-noise ratio is computed

as follows:

$$SNR(d, \gamma) = 228.6 + P_{TX} + g_A + (G/T)_{RX} - PL(d)$$
$$- L_{rain}(d, \gamma) - M_s(\gamma) - 10\log_{10}(B) \ (dB)$$
$$(19)$$

where

- P_{TX} is the power at the output of Tx Solid-State Power Amplifier (SSPA) including the OBO;
- g_A is the antenna gain, which is considered the same for the Tx and Rx;
- $(G/T)_{RX}$ is the figure of merit of the backhaul receiver;
- PL is the pathloss computed in LOS or NLOS scenarios using the parametrization indicated in Table 1;
- $L_{rain}(d, \gamma)$ is the rain attenuation, measured at a distance d that is exceeded with probability equal to γ;
- M_s is the shadow margin computed as: $M_s = \sigma_s Q^{-1}(\gamma)$ [30], where σ_s is the standard deviation of ϵ_s (*shadow standard deviation*) and $Q^{-1}(\cdot)$ is the inverse Gaussian Q-function;
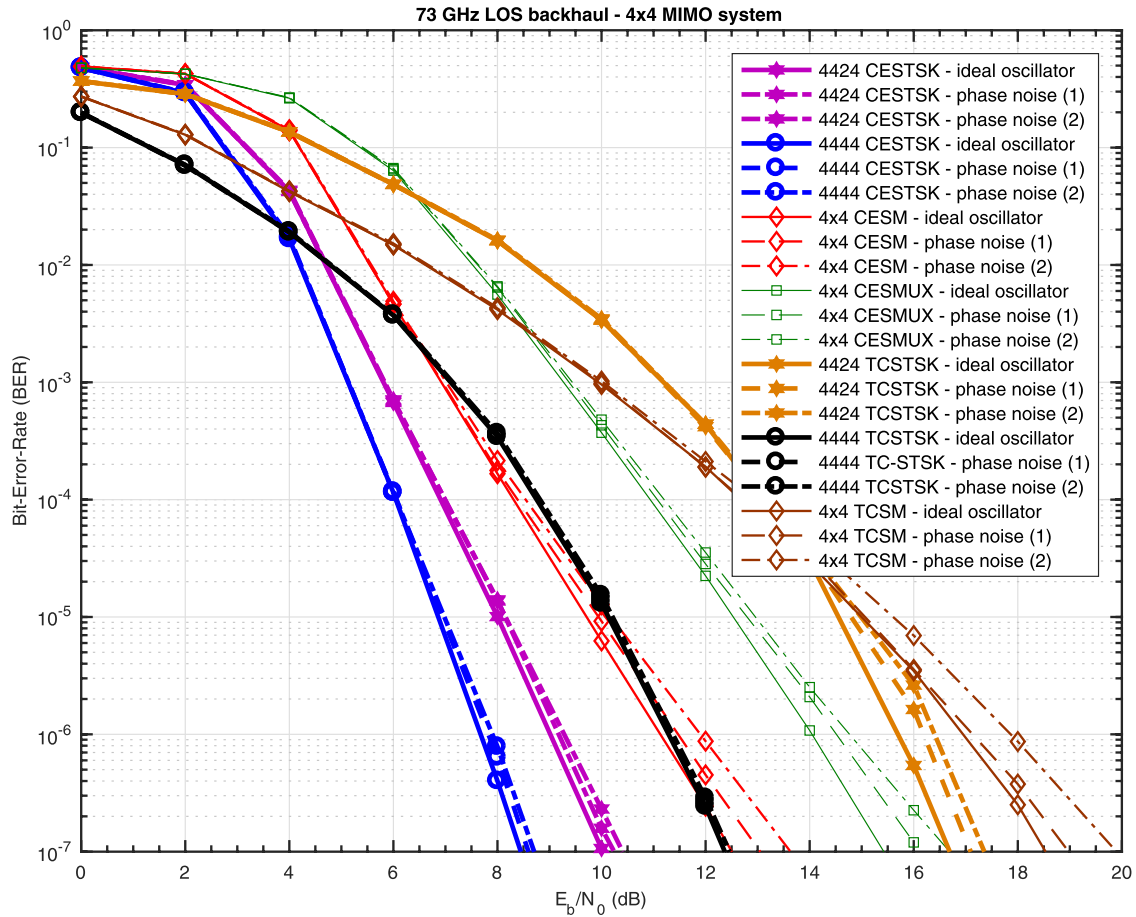- B is the occupied bandwidth slot, which is 500 MHz in our case.

FIGURE 10. BER vs. E_b/N_0 for 4x4 MIMO small-cell backhaul system: LOS channel state.
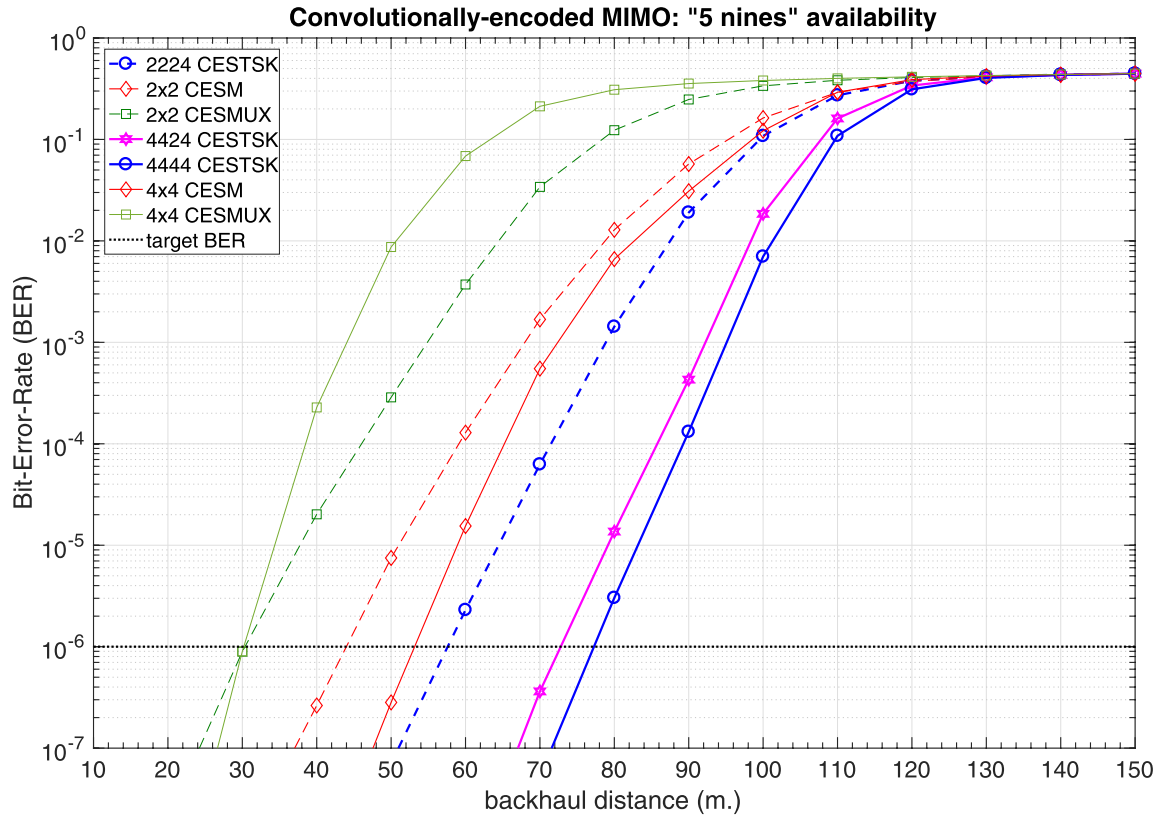
TABLE 5. Link budget parameters for mm-wave small-cell backhaul.

Parameter	Numerical value
P_{TX}	-8.5 dBW (inclusive of OBO)
g_A	24.5 dB
$(G/T)_{RX}$	24.38 dB/K
σ_s	8.0 dB (NLOS)
	5.8 dB (LOS)

In Table 5, the numerical values of the link budget parameters used for our simulations are presented. The value of P_{TX} has been taken from [38], including 8.5 dB of OBO needed to resort to the linear amplification zone. The other parameters have been computed on the basis of experimental data for the antenna gain, losses, noise figure and low-noise amplifier gain found in [4] and [39]. Finally, shadow standard deviation values have been experimentally measured in LOS and NLOS conditions in [4]. Additionally, we have used the complementary cumulative distribution functions of the rainfall intensity versus γ reported by Luini and Capsoni in [40]. The following values of rain attenuation have been obtained: $L_{rain} = 47.59\,dB/Km$ for $\gamma = 10^{-5}$,

$L_{rain} = 17.84\,dB/Km$ for $\gamma = 10^{-4}$, and $L_{rain} = 10.05\,dB/Km$ for $\gamma = 10^{-3}$. The attenuation due to oxygen absorption is well below 0.1 dB for small-cell distances and hence we neglected it.

The average BER of (18) has been plotted versus backhaul distance d for the CESTSK and TCSTSK techniques in Fig. 11 and Fig. 12, respectively, under "*five 9s*" availability requirements. The oscillator with the highest phase-noise PSD of [37], which was denoted as "phase-noise (2)" in the previous section, has been considered in these simulations in order to consider a "*worst case*" scenario, which is useful to derive a lower bound on the achievable coverage. As shown in Fig. 11 and Fig. 12, STSK offers the best coverage in all the considered situations. In general, the convolutionally-encoded MIMO transmission techniques are more robust than trellis-encoded techniques due to the fact that in this convolutionally coded systems, the channel coding is applied to the entire transmitted symbol block. The (4,4,2,4) CESTSK represents a good trade-off solution, providing a coverage of about 72 m. with a net spectral efficiency of 1 b/s/Hz. A slightly improved coverage has been provided by the (4, 4, 4, 4) CESTSK of about 77 m., while having half the

FIGURE 11. Average BER vs.backhaul distance *d* for convolutionally-encoded MIMO techniques and *"5 nines"* link availability.

TABLE 6. Computational complexity of the different MIMO techniques considered for mm-wave small-cell backhaul.

MIMO-OFDM technique	*Number of elementary operations*
STSK	$O\left(NTQ\left(4N+4L\right)\right)$ [17]
SM	$O\left(8N^2+4L\left(N+1\right)\right)$ [18]
SMUX	$O\left(L^N\left(8N^2+2N\right)\right)$ [35]

throughput of that for the (4, 4, 2, 4) CESTSK. A coverage of about 58 m. is provided by (2,2,2,4) CESTSK, which makes it suitable for scenarios where cell-sizes are considerably reduced and cost-effective MIMO systems are desired. On the other hand, the SM and SMUX considered in the simulations generally offer backhaul coverage of 50 m. or less, despite their increased throughput, which makes them not suitable for outdoor applications. It is worth noticing that under the link budget and availability constraints considered in these simulations, the barrier distance of 157 meters highlighted in Fig. 6 is not attained.

Therefore, in order to enhance backhaul coverage, we propose two solutions. The first one forecasts the use of almost linear amplifiers and antenna systems with higher gains, where in this work we have considered the horn antennas of [4]. However, this solution suffers from high monetary cost, energy consumption as well as Base Station size. The second solution is to relax the *"five 9s"* availability constraint, where due to the burst nature of backhaul traffic in small cellular systems, a continuous service availability may neither be useful nor advisable. Therefore, *"four 9s"* and *"three 9s"* availability could be enough for a satisfactory quality-of-service.

Hence, in order to appreciate the effect of relaxing the availability rate, we present the backhaul distances reachable by the different MIMO techniques, while keeping the same requirement of bit-error-rate equal 10^{-6}. These results are summarized by the bar plots of Fig. 13 and 14 for the convolutionally-encoded MIMO techniques and the trellis-coded MIMO techniques, respectively. As expected, relaxing the link availability rate, the achievable backhaul coverage improves for all techniques, but only CESTSK and (4, 4, 4, 4) TCSTSK can offer more than 100 m. of coverage with 99.9% availability. Additionally, the 4×4 CESM reaches 120 m. of backhaul coverage, but only in the *"three 9s"* case. Convolutionally-encoded SMUX, despite its high throughput, allows backhaul distances well below 100 m. in all the considered cases.
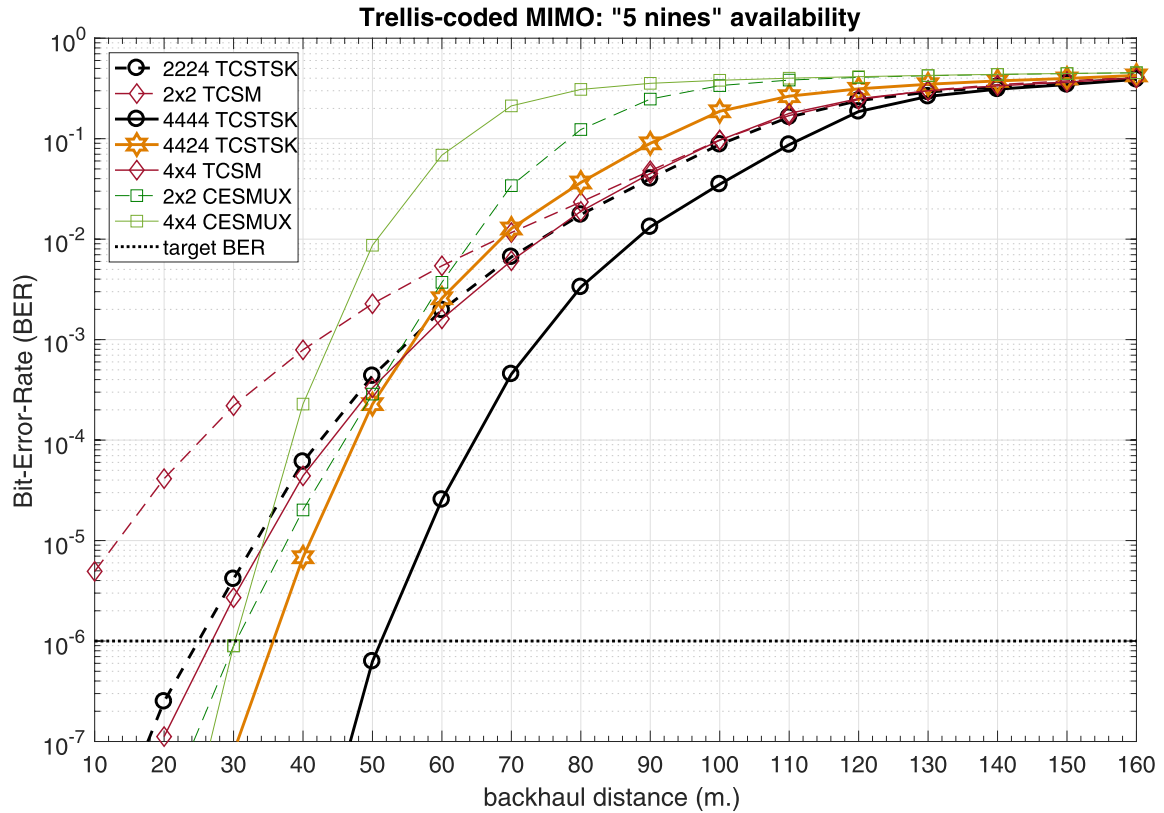
FIGURE 12. Average BER vs.backhaul distance *d* for trellis-encoded MIMO techniques and "*5 nines*" link availability.
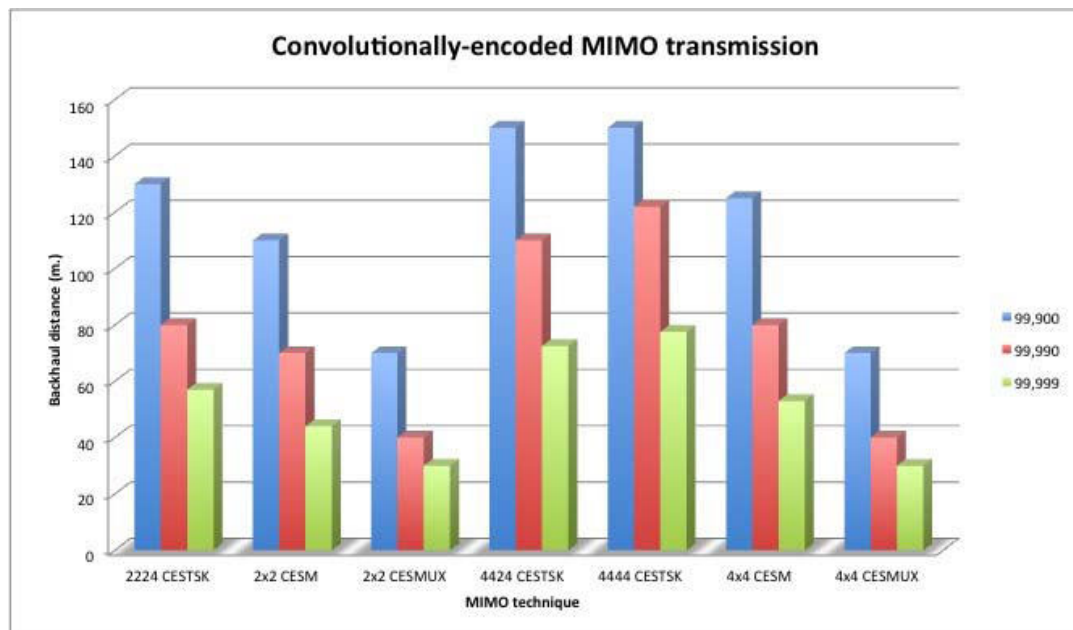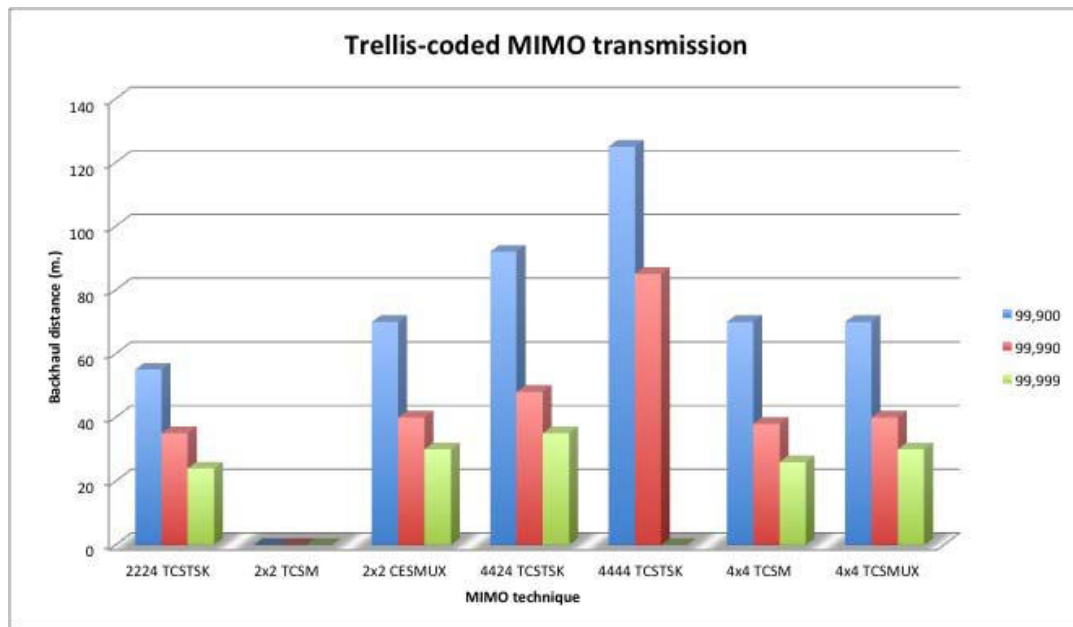

FIGURE 13. Backhaul coverage reachable by CESTSK and other convolutionally-encoded MIMO transmission techniques for different link availability rates and target BER equal to 10^{-6}.
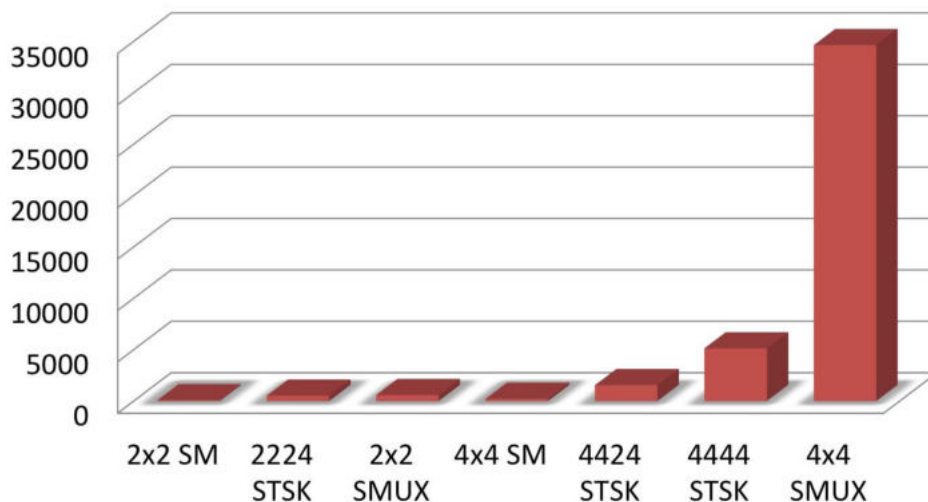
D. NOTES ABOUT COMPUTATIONAL COMPLEXITY

A crucial aspect in MIMO signal processing is related to the computational complexity. In Table 6 we show the computational complexity of OFDM-STSK FD-ML as well as that of the SM and SMUX techniques detection expressed in terms of the elementary operations required to estimate the

FIGURE 14. Backhaul coverage reachable by TCSTSK and other trellis-coded MIMO transmission techniques for different link availability rates and target BER equal to 10^{-6}.

FIGURE 15. Number of elementaryoperations required to demodulate a symbol block for different MIMO techniques considered for mm-wave backhaul.

symbol block transmitted over each subcarrier. The computational complexity of STSK is slightly increased with respect to that of SM, but consistently reduced when compared with that of SMUX, which becomes intractable when the number of MIMO antennas increases. The complexity of the different techniques is shown in the bar plot of Fig. 15 for different MIMO configurations.

VI. CONCLUSIONS

In this work, an innovative solution based on STSK and OFDM transmission is proposed for mm-wave small-cell backhaul in dense urban environments, where the presence of the line-of-sight between transmit and receive antennas is not guaranteed. Thanks to diversity exploited efficiently in time and space domain, STSK allows to greatly improve link performance and coverage under hostile propagation conditions compared to the state-of-the-art Spatial Modulation and Spatial Multiplexing. The gain of the STSK against SM techniques is attained at the cost of a reduced throughput and slightly increased computational complexity. In this paper, we have showed that the potential advantages of the STSK outweigh the drawbacks in the considered scenarios.

In our future work we will consider the design of countermeasures against non-linear distortions and phase noise in the STSK-OFDM system for millimeter wave communications. Additionally, we will consider the effect of channel estimation errors on STSK performance, with the consequential assessment of the computational and hardware cost that a robust channel estimator would involve on the backhaul transmission chain.

ACKNOWLEDGMENT

REFERENCES

[1] M. Agiwal, A. Roy, and N. Saxena, "Next generation 5G wireless networks: A comprehensive survey," *IEEE Commun. Surveys Tuts.*, vol. 18, no. 3, pp. 1617–1655, 3rd Quart., 2016.

[2] Y. Niu, Y. Li, D. Jin, L. Su, and A. V. Vasilakos, "A survey of millimeter wave communications (mmWave) for 5G: Opportunities and challenges," *Wireless Netw.*, vol. 21, no. 8, pp. 2657–2676, Nov. 2015.

[3] *Technical Requirements for Fixed Radio Systems Operating in the Bands 25.25–26.5 GHz and 27.5–28.35 GHz*, document SRSP-325.25, Federal Communications Commission, Office of Engineering and Technology, 2013.

[4] M. R. Akdeniz *et al.*, "Millimeter wave channel modeling and cellular capacity evaluation," *IEEE J. Sel. Areas Commun.*, vol. 32, no. 6, pp. 1164–1179, Jun. 2014.

[5] B. Farhang-Boroujeny and H. Moradi, "OFDM inspired waveforms for 5G," *IEEE Commun. Surveys Tuts.*, vol. 18, no. 4, pp. 2474–2492, 4th Quart., 2016.

[6] *Scenarios and Requirements for Small Cell Enhancement for E-URTA and E-UTRAN*, Eur. Telecommun. Standard Inst., Sophia Antipolis, France, 2014.

[7] X. Ge, S. Tu, G. Mao, and C. X. Wang, "5G ultra-dense cellular networks," *IEEE Trans. Wireless Commun.*, vol. 23, no. 1, pp. 72–79, Feb. 2016.

[8] V. Dyadyuk *et al.*, "A multigigabit millimeter-wave communication system with improved spectral efficiency," *IEEE Trans. Microw. Theory Techn.*, vol. 55, no. 12, pp. 2813–2821, Dec. 2007.

[9] C. Sacchi, C. Stallo, and T. Rossi, "Space and frequency multiplexing for mm-wave multi-gigabit point-to-point transmission links," in *Proc. IEEE Aerosp. Conf.*, Mar. 2013, pp. 1–10.

[10] P. W. Wolniansky, G. J. Foschini, G. D. Golden, and R. A. Valenzuela, "V-BLAST: An architecture for realizing very high data rates over the rich-scattering wireless channel," in *Proc. URSI Int. Symp. Signals, Syst., Electron. (ISSSE)*, Oct. 1998, pp. 295–300.

[11] I. Frigyes and L. Csurgai-Horvath, "From gigabit to multi-gigabit: mm waves in mobile networks' backhaul," in *Proc. IEEE Globecom Workshops*, Nov. 2009, pp. 1–6.

[12] M. Coldrey, J. E. Berg, L. Manholm, C. Larsson, and J. Hansryd, "Non-line-of-sight small cell backhauling using microwave technology," *IEEE Commun. Mag.*, vol. 51, no. 9, pp. 78–84, Sep. 2013.

[13] D. Cvetkovski, T. Halsig, B. Lankl, and E. Grass, "Next generation mm-Wave wireless backhaul based on LOS MIMO links," in *Proc. German Microw. Conf. (GeMiC)*, Mar. 2016, pp. 69–72.

[14] T. F. Rahman, C. Sacchi, and C. Stallo, "MM-wave LTE-A small-cell wireless backhauling based on TH-IR techniques," in *Proc. IEEE Aerosp. Conf.*, Mar. 2015, pp. 1–9.

[15] Z. Gao, L. Dai, D. Mi, Z. Wang, M. A. Imran, and M. Z. Shakir, "mmWave massive-MIMO-based wireless backhaul for the 5G ultra-dense network," *IEEE Wireless Commun.*, vol. 22, no. 5, pp. 13–21, Oct. 2015.

[16] L. Chen, F. R. Yu, H. Ji, V. C. M. Leung, X. Li, and B. Rong, "A full-duplex self-backhaul scheme for small cell networks with massive MIMO," in *Proc. IEEE Int. Conf. Commun. (ICC)*, May 2016, pp. 1–6.

[17] S. Sugiura, S. Chen, and L. Hanzo, "Coherent and differential space-time shift keying: A dispersion matrix approach," *IEEE Trans. Commun.*, vol. 58, no. 11, pp. 3219–3230, Nov. 2010.

[18] R. Y. Mesleh, H. Haas, S. Sinanovic, C. W. Ahn, and S. Yun, "Spatial modulation," *IEEE Trans. Veh. Technol.*, vol. 57, no. 4, pp. 2228–2241, Jul. 2008.

[19] P. Liu and A. Springer, "Space shift keying for LOS communication at mmWave frequencies," *IEEE Wireless Commun. Lett.*, vol. 4, no. 2, pp. 121–124, Apr. 2015.

[20] K.-C. Huang and Z. Wang, *Millimeter Wave Characteristics*. Hoboken, NJ, USA: Wiley, 2011, pp. 1–31.

[21] Intellimax. (2014). *Intellimax MB 2000 Mobile Backhaul, LTE North America*. [Online]. Available: http://americas.lteco nference.com

[22] Ceragon Corp. *Wireless Backhaul Solutions for Small Cells*, accessed on Mar. 28, 2017. [Online]. Available: https://www.winncom.com/ images/solutions/Ceragon_Small_Cell_Solution_Brief.pdf

[23] M. I. Kadir, S. Sugiura, S. Chen, and L. Hanzo, "Unified MIMO-multicarrier designs: A space–time shift keying approach," *IEEE Commun. Surveys Tuts.*, vol. 17, no. 2, pp. 550–579, 2nd Quart., 2015.

[24] S. Sugiura, "Dispersion matrix optimization for space-time shift keying," *IEEE Commun. Lett.*, vol. 15, no. 11, pp. 1152–1155, Nov. 2011.

[25] R. Mesleh, M. Di Renzo, H. Haas, and P. M. Grant, "Trellis coded spatial modulation," *IEEE Trans. Wireless Commun.*, vol. 9, no. 7, pp. 2349–2361, Jul. 2010.

[26] M. K. Samimi and T. S. Rappaport, "Local multipath model parameters for generating 5G millimeter-wave 3GPP-like channel impulse response," in *Proc. 10th Eur. Conf. Antennas Propag. (EuCAP)*, Apr. 2016, pp. 1–5.

[27] M. K. Samimi and T. S. Rappaport, "3-D statistical channel model for millimeter-wave outdoor mobile broadband communications," in *Proc. IEEE Int. Conf. Commun. (ICC)*, Jun. 2015, pp. 2430–2436.

[28] T. S. Rappaport, G. R. Maccartney, M. K. Samimi, and S. Sun, "Wideband millimeter-wave propagation measurements and channel models for future wireless communication system design," *IEEE Trans. Commun.*, vol. 63, no. 9, pp. 3029–3056, Sep. 2015.

[29] M. K. Samimi and T. S. Rappaport, "Ultra-wideband statistical channel model for non line of sight millimeter-wave urban channels," in *Proc. IEEE Global Commun. Conf.*, Dec. 2014, pp. 3483–3489.

[30] A. Goldsmith, *Wireless Communications*. New York, NY, USA: Cambridge Univ. Press, 2005.

[31] R. K. Crane, "Propagation phenomena affecting satellite communication systems operating in the centimeter and millimeter wavelength bands," *Proc. IEEE*, vol. 59, no. 2, pp. 173–188, Feb. 1971.

[32] *Millimeter Wave Propagation: Spectrum Management Implications*, Federal Commun. Commission, Office Eng. Technol., Washington, DC, USA, 1997.

[33] J. Tellado, L. M. C. Hoo, and J. M. Cioffi, "Maximum-likelihood detection of nonlinearly distorted multicarrier symbols by iterative decoding," *IEEE Trans. Commun.*, vol. 51, no. 2, pp. 218–228, Feb. 2003.

[34] R. M. Rao and B. Daneshrad, "Analog impairments in MIMO-OFDM systems," *IEEE Trans. Wireless Commun.*, vol. 5, no. 12, pp. 3382–3387, Dec. 2006.

[35] Y. S. Cho, J. Kim, W. Y. Yang, and C. G. Kang, *MIMO-OFDM Wireless Communications With MATLAB*. Hoboken, NJ, USA: Wiley, 2010.

[36] S. Trotta *et al.*, "A V and E-band packaged direct-conversion transceiver chipset for mobile backhaul application in SiGe technology," in *Proc. 44th Eur. Microw. Conf.*, Oct. 2014, pp. 1655–1658.

[37] Z. Huang, H. C. Luong, B. Chi, Z. Wang, and H. Jia, "A 70.5-to-85.5 GHz 65 nm phase-locked loop with passive scaling of loop filter," in *IEEE Int. Solid-State Circuits Conf. (ISSCC) Dig. Tech. Papers*, Feb. 2015, pp. 1–3.

[38] K. Tsukashima, A. Otsuka, M. Kubota, T. Tokumitsu, and S. Ogita, "An E-band 1 W-class PHEMT power amplifier MMIC," in *Proc. 10th Eur. Microw. Integr. Circuits Conf. (EuMIC)*, Sep. 2015, pp. 9–12.

[39] O. Katz *et al.*, "High-power high-linearity SiGe based E-BAND transceiver chipset for broadband communication," in *Proc. IEEE Radio Freq. Integr. Circuits Symp.*, Jun. 2012, pp. 115–118.

[40] L. Luini and C. Capsoni, "Estimating the spatial cumulative distribution of rain from precipitation amounts," *Radio Sci.*, vol. 47, no. 1, p. RS1005, 2012.

CLAUDIO SACCHI (SM'07) received the Laurea degree in electronic engineering and the Ph.D. degree in space science and engineering from the University of Genoa, Italy, in 1992 and 2003, respectively. Since 2002, he has been an Assistant Professor with the Faculty of Engineering, University of Trento, Italy. He has authored or co-authored over 90 papers published in international journals and conferences. The research interests are mainly focused on wideband mobile and satellite transmission systems based on space, time and frequency diversity, MIMO systems, array processing, multi-rate and multi-access wireless communications, EHF broadband aerospace communications, software radio and cognitive radio, and radio communications for emergency recovery applications. He is a member of the IEEE ComSoc, the IEEE Broadcast, and the IEEE AESS society. In 2011, he was a Guest Editor of the special issue of proceedings of the IEEE Aerospace Communications: History, Trends and Future.

TALHA FAIZUR RAHMAN received the B.S. degree in electrical engineering from the Islamic University of Technology, Dhaka, Bangladesh, in 2007, and the M.S. degree in telecommunication engineering and the Ph.D. degree from the University of Trento, Trento, Italy, in 2012 and 2015, respectively. He served as a Lecturer for two years with the Center for Advanced Studies in Telecommunications, COMSATS Institute of Information Technology, Islamabad, Pakistan. His research activities include radio resource management, MIMO, co-operative communication, and cognitive radios.

IBRAHIM A. HEMADEH received the B.Eng. degree (Hons.) in computer and communications engineering from the Islamic University of Lebanon in 2010 and the M.Sc. degree (Hons.) in wireless communications from the University of Southampton, U.K., in 2012, where he is currently pursuing the Ph.D. degree in wireless communications, under the supervision of Prof. L. Hanzo and Dr. M. El-Hajjar. His research interests mainly include millimeter wave communications, multifunctional MIMO, and multi-user MIMO.

MOHAMMED EL-HAJJAR received the Ph.D. degree in wireless communications from the University of Southampton, U.K., in 2008. He joined Imagination Technologies, as a Design Engineer, where he was involved in designing and developing imagination's multi-standard communications platform, which resulted in three patents. He is currently an Associate Professor with the Department of Electronics and Computer Science, University of Southampton. He has authored a Wiley–IEEE book and in excess of 80 journal and conference papers. His research interests include the development of intelligent communications systems, energy-efficient transceiver design, cross-layer optimization for large-scale networks, MIMO, millimeter wave communications, and radio over fiber network design. He was a recipient of several academic awards.

• • •